Developments in the Built Environment 17 (2024) 100288

Contents lists available at ScienceDirect

Developments in the Built Environment

journal homepage: www.sciencedirect.com/journal/developments-in-the-built-environment

Effects of pre-cracked width and seawater erosion on the cracking behavior of SFRC beams with BFRP bars subjected to cyclic loading

Haitang Zhu [a,b], Wencheng Duan [c], Zongze Li [b,*], Zemin Li [b], Xiangming Zhou [d], Qingxin Meng [e]

[a] School of Civil Engineering, Henan University of Engineering, Zhengzhou, 451191, China
[b] School of Civil Engineering, Zhengzhou University, Zhengzhou, 450001, China
[c] China Water Resources Beifang Investigation and Research Co Ltd, Tianjin, 300222, China
[d] Department of Civil & Environmental Engineering, Brunel University London, Uxbridge, UB8 3PH, UK
[e] China Construction Seventh Engineering Division. Corp. LTD, Zhengzhou, 450004, China

ARTICLE INFO

Keywords:
Pre-cracked width
Seawater corrosion
SFRC beams
Cracking behavior
BFRP bars

ABSTRACT

This study aims to explore the effects of various pre-cracked widths, seawater erosion and BFRP reinforcement ratios on the cracking behavior of steel fiber reinforced concrete (SFRC) beams with Basalt Fiber Reinforced Polymer (BFRP) bars subjected to cyclic loading. Pre-cracked beams were made by applying loads to obtain a predetermined crack width, such as 0.02 mm, 0.2 mm, and 0.4 mm crack widths. Eleven beams were poured and tested by a four-point bending load under cyclic loading. The crack pattern and load-crack width curves of beams were drawn and analyzed. The effects of pre-cracked width, seawater erosion, and BFRP reinforcement ratio on crack behaviors of beams were investigated and discussed. The results showed that the tensile strength of BFRP bars degenerated after seawater corrosion, and its degradation rates increased with the increase of diameter. The failure mode of beams after seawater erosion may transform from concrete crushing failure to BFRP tensile failure; The maximum crack width of all beams under service load was less than 0.5 mm. Increasing the BFRP reinforcement ratio can significantly improve the crack resistance of beams, but pre-cracked width and seawater erosion had adverse effects on the crack behavior. Existing codes overestimated the crack width of SFRC beams reinforced with BFRP bars. Finally, a new calculation model of crack width of SFRC beams with BFRP bars after seawater corrosion was proposed, and its results were closer to the experimental results.

1. Introduction

Corrosion of steel bars in marine environments has become a major factor in shortening the lifespan of offshore reinforced concrete (RC) structures, resulting in billions of dollars in economic losses due to annual maintenance and reconstruction costs (Li et al., 2022; Demis and Papadakis, 2019). Fiber reinforced polymer (FRP) bars are increasingly widely used in offshore reinforced concrete structures due to their excellent corrosion resistance, lightweight, and high tensile strength (Hu et al., 2019; Zhu et al., 2020). FRP are usually divided into Basalt Fiber Reinforced Polymer (BFRP), Glass Fiber Reinforced Polymer (GFRP), Aramid Fiber Reinforced Polymer (AFRP) and Carbon Fiber Reinforced Polymer (CFRP) due to the different reinforcement materials (Hamed et al., 2018). Among them, CFRP has the best mechanical properties (Deng et al., 2022), but its high cost limits its applications in engineering structures. In contrast, BFRP (Liu et al., 2021) and GFRP (Wu et al., 2023) have low production costs and excellent corrosion resistance, making them relatively widely used in civil engineering. The retention rate of tensile strength of GFRP bars decreases from 100% to 82.6% after exposing alkaline environment for 300 days. and the corrosion of the GFRP bars can be accelerated by pre-cracks in a strongly, under the same exposure time, a single pre-crack reduces the tensile strength of GFRP-RC by 19.5% (Wu et al., 2022) , but BFRP bars have better alkali resistance, chemical stability. More importantly, the reinforcing fiber of BFRP bars is made by melting basalt stones, which has little impact on the environment (Su et al., 2022a; Dong et al., 2020). Overall, BFRP bars are regarded as a promising alternative to replace steel bars in RC structures exposed to extremely corrosive environments.

Compared with RC structures, FRP-RC structures typically have wide cracks, large deformations, and poor ductility due to the low elastic modulus of FRP bars and poor bonding performance with concrete (Ribeiro and Diniz, 2013). Existing studies (Ngo et al., 2020; Hou et al.,

* Corresponding author.
E-mail address: zzulizongze@zzu.edu.cn (Z. Li).

https://doi.org/10.1016/j.dibe.2023.100288
Received 27 August 2023; Received in revised form 7 November 2023; Accepted 24 November 2023
Available online 29 November 2023

2021; Gribniak and Sokolov, 2023) had proven that using steel fiber reinforced concrete (SFRC) was the best way to solve the problems of FRP-RC structures. Although FRP bars have excellent corrosion resistance, their mechanical properties will deteriorate after long-term service in harsh environments. Wang et al. (2018) investigated the influence of seawater sea sand concrete environment and sustained load on the degradation of FRP bars, it was found that the strength remained 92.9 %, 78.9 %, and 43.2 % for BFRP bars after exposed to 25 °C environments for 63 days. Xiao et al. (2021) conducted an electrochemical accelerated corrosion test of steel-FRP composite bar (SFCB), and the results showed that the corrosion rate of ordinary steel reinforcement was 31.71 %. The corrosion rates of a carbon- and a glass-type SFCB are less than 1/10 (2.92 %) and 1/100 (0.3 %) that of an ordinary steel bar, respectively. Other literature had also shown that FRP bars exhibited strength degradation during long-term service in harsh environments (Almusallam et al., 2006; Guo et al., 2022; Liang et al., 2021), which can lead to durability issues in FRP-RC structures. Li (Li et al., 2021)summarized the quasi-static tensile properties of FRP composites after exposure in simulated seawater environment, it was found that the degradation degree of FRP composites increased with the exposure time, temperature, stress level and alkalinity/salinity of the immersion solution.

The seawater environment not only effect the mechanic performance of BFRP bars, but also have influence in the flexure performance of SFRC structure reinforced with FRP bars. The flexural behaviors of SFRC beams with FRP bars in marine environments was related to various factors, such as steel fiber content, BFRP reinforcement ratio, seawater erosion age (Lu et al., 2023a; Dong et al., 2022), and pre-cracked width (Wu et al., 2022; He et al., 2017). Lu et al. (2023b) investigated the durability of BFRP-RC concrete beams in simulated seawater, and the results showed that the flexural strength of the BFRP-RC beams after soaking in seawater for 180 days and 360 days decreased to 60% and 47% of the control specimen, respectively. Su et al. (2022b) founded that as the corrosion age increased, the bond strength between BFRP bars and surrounding concrete decreased, additionally, carbon nanotube modification can effectively slow down the degradation rate of tensile strength of BFRP bars. Wang (Wang et al., 2023) founded continuous loading and exposure to chloride environments had a negative impact on pre-stress loss of GFRP-RC beams, but the ultimate flexural strength of the conditioned beams with over-reinforcement did not decrease significantly due to their failure controlled by the concrete. Yuan (2019) studied the flexural performances of sea sand concrete beams reinforced with FRP bars. Compared with ordinary FRP-RC beams, sea sand reinforced concrete beams experience a transition from balanced-reinforcement to a less-reinforcement failure, resulting in a decrease in ultimate load and an increase in maximum crack width. Although previous studies had confirmed the degradation of mechanical performances of FRP-RC beams in marine environments and achieved relevant results, there was a lack of research on the degradation of the mechanical performances of SFRC beams with FRP bars. More importantly, the FRP-RC structures often works with cracks during service, which will exacerbate the cracking of the mechanical performances of beams. Therefore, considering the actual stress characteristics of the structures, it is of great engineering value to study the crack behaviors of pre-cracked SFRC beams with FRP bars in marine environments.

This study aimed to investigate the influence of pre-cracked width, erosion age and BFRP reinforcement ratio on the cracking behavior of SFRC beams with BFRP bars subjected to cyclic loading. To achieve this objective, eleven SFRC beams with BFRP bars were poured and tested through a four-point bending test under cyclic loading. The load, deformation, crack width, and crack development of the beams during the loading process were recorded and investigated. Revealed the influence of variables on failure mode, characteristic load, crack development, and crack width of beams. Finally, based on the ACI 440.1R-15 (ACI Committee, 2015) code, a new calculation method for the maximum crack width of SFRC beams with FRP bars considering the effects of steel fiber, erosion time, and pre-cracked width was proposed. Simultaneously compare the calculation results of existing codes (ACI Committee, 2015; Technical code for infrastructure application, 2010; Recommendation for design and construction, 1997) and new models with experimental results, and the new model results were closer to the experimental results.

2. Experimental program

2.1. Materials

2.1.1. BFRP bars

The BFRP bars with diameters of 12 mm and 14 mm used in the study were produced by Chinese GMV Ltd. According to the ACI 440.3R-12 (ACI Committee, 2012) code, the mechanical properties of the BFRP bars before and after corrosion were tested, including their ultimate strength, rupture strain, and elastic modulus. Fig. 1 shows the tensile testing device for BFRP bars. Table 1 lists the mechanical properties of BFRP bars.

2.1.2. SFRC

According to the CECS 38–2004 (Technical specification for fiber reinforced, 2004) code, the mix design of SFRC was obtained, as shown in Table 2. The type PO 42.5 cement was utilized as the cementitious material. Natural crushed stone having particle sizes of 5~20 mm and river sand with a fineness modulus of 2.59 were used as coarse and fine aggregates, respectively (see Fig. 3). The end-hook shaped steel fiber with a diameter of 0.55 mm and a length of 35 mm was used, and its tensile strength was 1345 MPa, and Young's modulus was 200 GPa (as shown in Fig. 3). The polycarboxylate superplasticizer was added to guarantee favorable workability of the SFRC.

2.2. Specimen design and experiment setup

Eleven SFRC beams with BFRP bars were poured, and their design details are summarized in Table 3. The beams mainly included three variables, such as BFRP reinforcement ratios (0.56%, 0.77%, 1.15%, and 1.65%), erosion age (0d, and 365d), and pre-cracked widths (0.02 mm, 0.2 mm, and 0.4 mm). The geometric dimensions of all beams were 2100 mm in length (l), 150 mm in width (b), and 300 mm in depth (h), as shown in Fig. 2. Two steel bars of 6 mm in diameter were used as the top frame reinforcement, and the steel stirrups with diameters of 10 mm were placed at 75 mm spacing in the shear span. The concrete cover was 15 mm. To label the test specimens, a test specimen-identifying system was employed. The code name for each beam specimen was represented as C (or N)-m-n, where the letters C or N indicated whether a SFRC beam specimen underwent artificial seawater corrosion or not, respectively. The number next to C or N, "m," indicates the tensile reinforcement ratio in percentage, while the final number "n" represents the pre-cracked width (in millimeters) of beams in the pure bending span. For instance, Beam C-0.77-0.2 points to a beam with a reinforcement ratio of 0.77% and pre-cracked width of 0.2 mm, subjected to artificial seawater corrosion for 1 year.

All beams were tested by Hydraulic Press Machine (HPM) with a loading capacity of 2000 kN at Zhengzhou University (as shown in Fig. 4). The beams were supported on a steel frame, and the load from the actuator was applied to the beams through a load distribution steel beam. A linear variable differential transducer (LVDT) was mounted in the middle of the beams, the location was shown in Fig. 2, which recorded the deformation of the beam automatically through a data acquisition system. The crack widths were recorded by a crack observer (ZBL-F120) during the test. The test equipment (HPM, LVDT, and crack observer ZBL-F120) were shown in Fig. 4.

The loading method of pre-cracked beams was mainly divided into two processes, including pre-cracked loading and formal loading. For the pre-crack loading process, this study adopted a load control method

Fig. 1. Testing BFRP bars.

Table 1
Mechanical properties of the BFRP bars.

Sample designation	Cross sectional area A (mm^2)	Modulus of elasticity E_f (GPa)		Ultimate tensile stress f_{fu} (MPa)		FRP rupture strain	
		Before corrosion	After corrosion	Before corrosion	After corrosion	Before corrosion	After corrosion
BFRP12	113.04	43.26	39.4	1034.1	926.9	0.024	0.023
BFRP14	153.86	41.79	38.2	1025.6	910.8	0.024	0.024

Table 2
Concrete mix proportions (in kg/m^3).

Water	Cement	Fine aggregate	Coarse aggregate	Steel fiber	Polycarboxylate superplasticizer
164	529	706	1026	78.5	5.82

of increasing by 5 kN until the maximum crack width reached the target value, such as crack widths of 0.02 mm, 0.2 mm, and 0.4 mm. When the maximum crack width of the beam reached the target value, we unload and placed the beam in artificial seawater for erosion testing. The beam underwent the second stage of formal loading tests after one year of erosion. This formal loading was carried out by a displacement control method with the controller increasing 6 mm, and three cycles of loading and unloading were carried out during each increase of displacement, as shown in Fig. 5. For other beams without cracks, there was only a formal loading process.

2.3. Simulated seawater environment

Artificial seawater was prepared in accordance with ASTM D1141-98 (Standard practice for preparation of). The salt solution composition included 28.22 g NaCl, 2.40 g $MgCl_2$, 3.44 g $MgSO_4$, 1.23 g $CaCl_2$, 0.26 g $NaHCO_3$, and 0.76 g KCl in 1 L deionized water. The prescribed artificial seawater was poured into an immersion pool where SFRC beams and concrete cube specimens had already been placed. However, the solution substance content changed over time, necessitating monthly monitoring through chloride Selective electrode. The simulated seawater solution was thus replaced monthly according to the monitored results. Following the specified immersion time, the specimens were air-dried for two days before testing. Fig. 6 depicts the SFRC beams with Basalt bars, cubes, and bars in the immersion pool.

3. Results and discussion

3.1. Mechanical properties concrete and BFRP bars

As shown in Table 1, there was a significant decrease in the tensile strength and elastic modulus of BFRP bars after being immersed in artificial seawater for one year. For BFRP bars with a diameter of 12 mm, the tensile strength decreased from 1034.1 MPa to 926.9 MPa after being immersed in artificial seawater for one year, and the elastic modulus decreased from 43.26 GPa to 39.4 GPa. The degradation rate of tensile strength was 10.4%, which was higher than the degradation rate of elastic modulus of 8.9%. The reason was that the large amount of free water molecules and hydroxide ions were generated in concrete due to seawater penetration and cement hydration in humid and marine environments, which entered the interior of the FRP bars through penetration and capillary to hydrate the hydrophilic groups and water-soluble substances in the resin matrix, resulting in the hydrolysis of

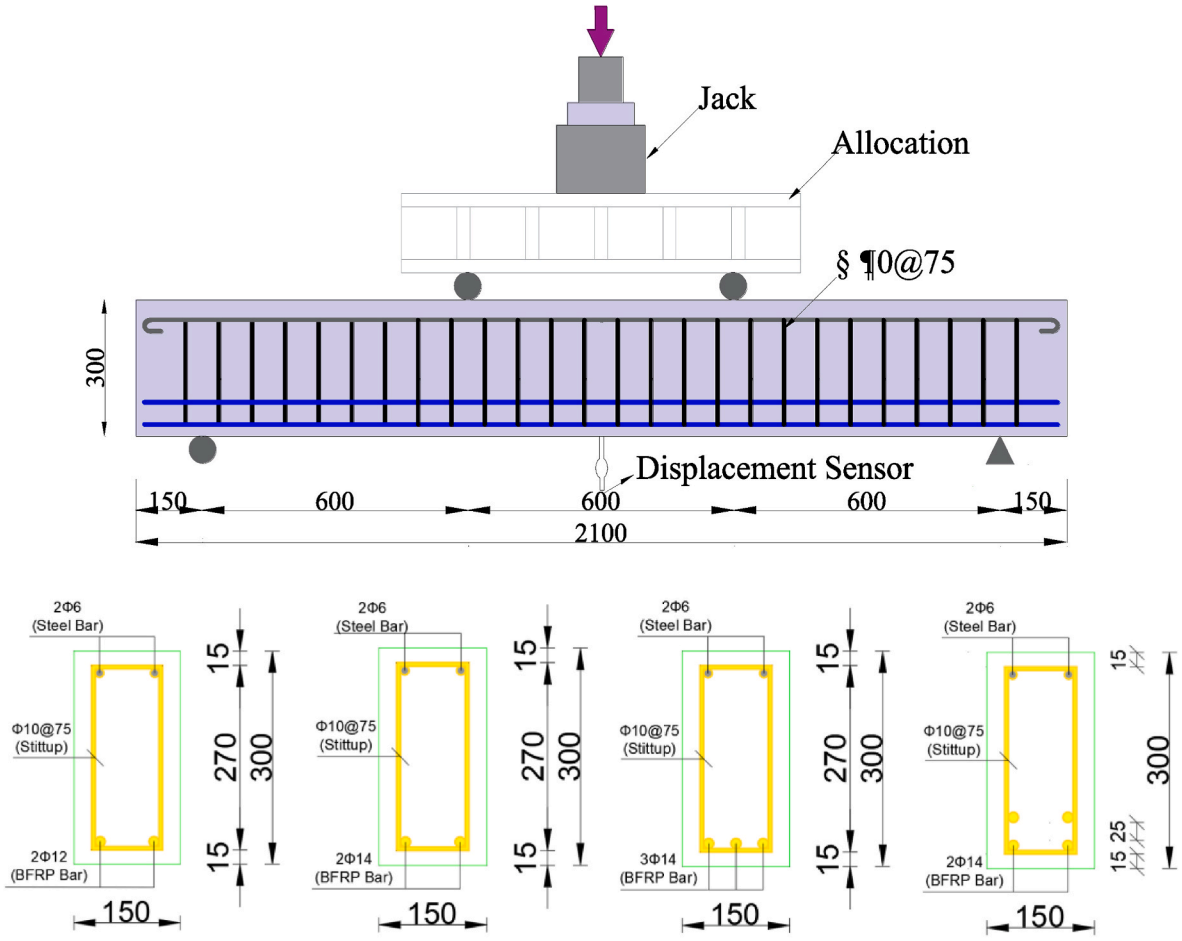

Fig. 2. Details and dimensions of the test beams (unit: mm).

Fig. 3. (a) Steel fibers, (b) Coarse aggregates and (c) Fine aggregates.

the resin and deboning of the fiber and the resin. In addition, the swelling of the resin provided a channel for the flow of the solution, In the absence of resin protection, the Si-O-Si bond in the exposed fiber was destroyed by the hydroxide, causing the Si-O-Si bonds in the fibers to be directly exposed to the solution by hydroxides and accelerating their destruction, leading to a damage to the FRP bars and even fiber breakage, affecting the mechanical properties of the FRP bars. Similar results were observed in BFRP bars with a diameter of 14 mm. Significantly, the diameters of FRP bars also affected the degradation rate of tensile strength. The tensile strength of BFRP bars with a diameter of 14 mm was reduced from 1025.6 MPa to 910.8 MPa, but its strength degradation rate was 11.2%, which was higher than that of BFRP bars with a diameter of 12 mm. This was because the outermost fiber wrapped in BFRP bars was exposed increased stress-induced failure, causing the breakage to spread to the inside in an instant (Ali et al., 2020; Feng et al., 2022). The literatures (Hollaway, 2010; Benmokrane et al., 2017) also found similar results.

As shown in Table 3, the compression strength of concrete after immersing in artificial seawater for 365d increased by 15.9% compared with concrete that only curing for 28d. The reason was the curing time was increased, the hydration reaction of cement was more sufficient, the internal porosity of the concrete was reduced, so the strength increased.

Table 3
Design details of beams.

Specimen	Flexural reinforcement		f_{cu}	d_c	ρ_f	ρ_b	ρ_{sf}	Pre-cracked width	Corrosion time	Mechanical properties of concrete
	Type	A_f (mm)^2	(MPa)	(mm)	(%)	(%)	(%)	(mm)	(year)	f_{cu} (MPa)
C-0.56-0	BFRP	226.19	60	267	0.56	0.32	1	–	1	77.24
C-0.77-0	BFRP	307.88	60	268	0.77	0.33	1	–	1	87.50
C-1.15-0	BFRP	461.81	60	268	1.15	0.35	1	–	1	83.37
C-1.65-0	BFRP	615.75	60	248.5	1.65	0.35	1	–	1	86.61
C-0.77-0.02	BFRP	307.88	60	268	0.77	0.33	1	0.02	1	83.13
C-0.77-0.2	BFRP	307.88	60	268	0.77	0.33	1	0.2	1	81.69
C-0.77-0.4	BFRP	307.88	60	268	0.77	0.33	1	0.4	1	84.17
N-0.56-0	BFRP	226.19	60	267	0.56	0.32	1	–	0	60.16
N-0.77-0	BFRP	307.88	60	268	0.77	0.33	1	–	0	74.99
N-1,15-0	BFRP	461.81	60	268	1.15	0.35	1	–	0	76.06
N-1.65-0	BFRP	615.75	60	248.5	1.65	0.35	1	–	0	76.47

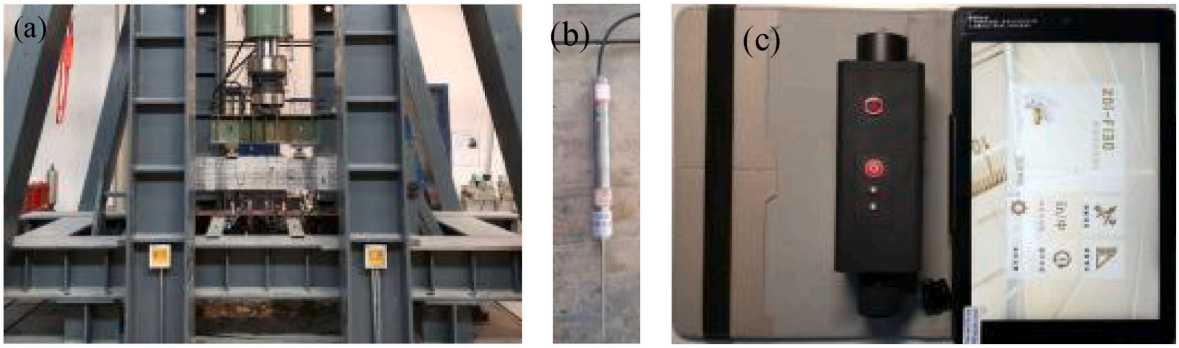

Fig. 4. (a) HPM, (b) LVDT and (c) Crack observer.

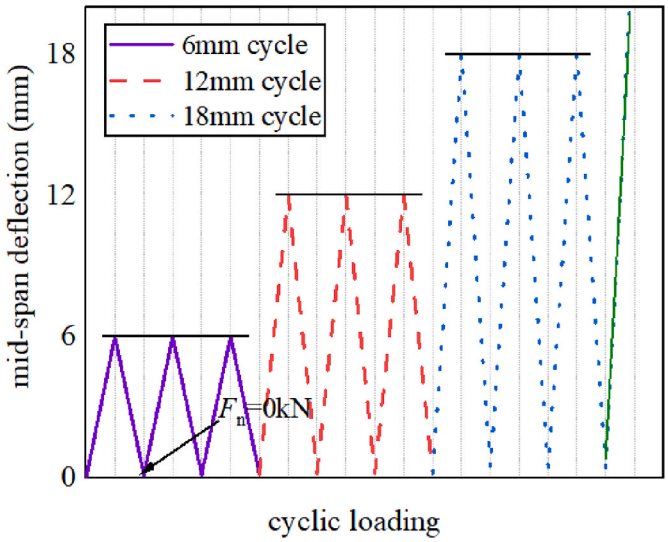

Fig. 5. Cyclic loading regime.

Fig. 6. Immersion photograph.

3.2. Crack propagation and characteristic load

3.2.1. Failure mode

FRP bars have a lower elastic modulus, resulting in the design of FRP-RC beams being usually controlled by the service performances of the beams, such as the crack width. The CSA S806–12 (Standard, 2012) suggests that the service load (L_s) is 0.3 times of the ultimate load (L_u) of FRP-RC beams. The cracking load (L_{cr}) refers to the load when a crack first appears in the tensile zone or the load corresponding to tensile strain of the FRP bars suddenly increases. The stabilized load (L_{st}) was defined as the load when no new crack appears in the pure bending zone of the beams. Table 4 shows the cracking load (L_{cr}), ultimate load (L_u), failure mode, number of cracks, crack spacing, maximum crack depth, and maximum crack width of SFRC beams with BFRP bars. The final crack distribution of the beams was depicted in Fig. 7. As shown in Table 5 and Fig. 7, two failure modes were observed in the tested beams: concrete compression failure (CF) and BFRP bars tensile failure (TF). There were significant differences in crack development of beams between the two failure modes. For the beams with TF, when load reached to the cracking load (L_{cr}), the vertical flexural cracks were generated in the pure bending region of beams, and the depth had quickly developed to 1/3 h. With the increment of the load, the flexural crack number, crack depth and crack width expanded quickly. The crack number no longer changed and the growth rate of crack depth slowed down after stabilized load (L_{st}), but the growth rate of crack width accelerated. As the load further increased, the strain of BFRP bars increased smartly, reaching its ultimate tensile strain, leading to a rapid decrease in the bearing capacity of the beams. The beams with TF was prone to brittle failure, which seriously affected the safety of the structures. Therefore, the beams with TF should be avoided in design (Wang et al., 2022). Unlike the crack development of beams with TF, the crack depth of beams with CF only developed to 1/4 h and 1/2 h at L_{cr} and L_{st}, respectively, which was lower than that of beams with TF. More importantly, horizontal cracks began to appear in the concrete

Table 4
Detail of crack propagation and characteristic load.

Spec.	L_{cr}	L_{st}	L_u	Failure mode	Number. of cracks		Crack spacing (mm)		Maximum crack depth (mm)			Maximum crack width (mm)			
					L_{cr}	L_{st}	L_{cr}	L_{st}	L_{cr}	L_{st}	L_u	L_{cr}	L_s	L_{st}	L_u
C-0.56-0	37	80	147	TF	3	7	117	129	123	268	279	0.04	0.36	0.62	3
C-0.77-0	38	87	193	TF	3	6	123	130	105	235	246	0.04	0.36	0.66	2.53
C-1.15-0	40	122	256	TF	4	7	103	98	93	203	233	0.05	0.31	0.42	1.7
C-1.65-0	47	160	303	TF	4	9	99	99	90	188	300	0.02	0.29	0.42	1.3
C-0.77-0.02	–	88	190	TF	–	8	–	145	–	258	271	–	0.37	0.67	3.4
C-0.77-0.2	–	85	160	TF	–	5	–	221	–	242	267	–	0.32	1.4	3.6
C-0.77-0.4	–	84	130	TF	–	6	–	230	–	235	282	–	0.35	1.8	5
N-0.56-0	46	106	173	TF	3	5	69	139	103	180	271	0.02	0.38	0.72	5.3
N-0.77-0	47	101	243	TF	3	5	79	115	99	167	251	0.02	0.40	0.70	5.2
N-1.15-0	50	140	337	CF	4	9	64	95	74	153	300	0.03	0.38	0.68	3.5
N-1.65-0	53	229	356	CF	5	9	62	92	66	119	300	0.02	0.40	0.63	2.9

compression zone when the beam was about to fail. As the load further increased, multiple horizontal cracks gradually formed through cracks, and the strain at the edge of the concrete in the compression zone reached its limit, resulting in a decrease in the bearing capacity of the beams. The beams with CF exhibited good ductility, so existing codes recommend that FRP-RC structures should be designed with a concrete crushing failure mode. This implied that failure mode was associated with the BFRP reinforcement ratio, a beam with a higher reinforcement ratio have a stronger ability to restrain the concrete surrounding the BFRP bars and a higher tensile bearing capacity. It is interesting to note that the failure modes of beams C-1.15-0 and C-1.65-0 had changed from CF to TF on the score of seawater corrosion, which decrease the tensile strength and elastic modulus of BFRP bars.

3.2.2. Load analysis

As shown in Table 4, the crack load was related to corrosion environment, but not to the BFRP reinforcement ratio. The crack loads of corrosion beams were averagely decreased to 21% comparing with no-corrosion beams. Seawater corrosion had a negative impact on the concrete tensile strength, causing the reduction of crack load. However, the stabilized load and ultimate load were related to BFRP reinforcement ratio, corrosion environment and pre-cracked width. With the increase of BFRP reinforcement ratio, the stabilized load and ultimate load were improved, which was suit for beams subjected to seawater erosion. In addition, the influence of BFRP reinforcement ratio on the ultimate load of beams with low BFRP reinforcement ratio was higher than that of beams with high BFRP reinforcement ratio. When the BFRP reinforcement ratio increased by 37.5% from 0.56%, the ultimate load increased by 31.3%, and when the BFRP reinforcement ratio increased by 43.5% from 1.15%, the ultimate load only increased by 18.4%. For the broken beams with TF, the ultimate load of the beams was directly related to the BFRP reinforcement ratio, while for the beams with CF, increasing the BFRP reinforcement ratio can indirectly increase the height of the concrete compression area, thus increasing the ultimate of the beams, so the level of BFRP reinforcement ratio had different impacts on the ultimate load of beams. What's more, the stabilized load and ultimate load of SFRC beams with BFRP bars after soaking in simulate seawater solution for one year would reduce by 26% and 23%, respectively. The stabilized load and ultimate load of beam N-1.65-0 reduced by 43% and 17% comparing the beam C-1.65-0, respectively. It was noticed that the stabilized load of the pre-cracked beams did not change much compared with the normal beam, but the ultimate load decreased significantly. The ultimate load decreased by 1.5%, 20.6% and 48.5% when increased the pre-cracked widths from 0 to 0.02 mm, 0.2 mm and 0.4 mm, respectively. Due to the larger the pre-width, the larger the initial residual crack of the beams, and the greater the impact on of seawater corrosion on the beams, resulting in an increase in the width of cracks under the same load, an increase in the strain of the BFRP bars, a shorter test time, and an acceleration in the destruction process of the tested beams.

3.2.3. Crack depth and crack width

The data in Table 4 shows that the crack depth of SFRC beams with BFRP bars was closely related to the working environment and BFRP reinforcement ratio. The crack depth of beams after soaking in simulate seawater for one year would increase by 17%, 21% and 7% under L_{cr}, L_{st} and L_u, respectively. This result can be explained that seawater corrosion reduced the tensile strength of concrete and BFRP bars, resulting in an accelerated crack development rate, and leaded to deeper crack depths in corrosion beams than that in normal beams. With the increase of BFRP reinforcement ratio, the crack depth reduced before L_{st}, for example, the crack depth of beam C-0.56-0 was 36.7% and 42.6% larger than that of beam C-1.65-0 under L_{cr} and L_{st}. Because increasing the BFRP reinforcement ratio could help improve the bond between concrete and BFRP bars, and inhibit the development of cracks. The pre-cracked width had no significant impact on the crack depth before the stabilized load, but had a significant impact under the ultimate load. Compared with undamaged beams, the crack depth of beams with pre-cracked widths of 0.02 mm, 0.2 mm and 0.4 mm at L_{st} increased by 9%, 3% and 0%, while, the crack depth at L_u increased by 10%, 9% and 14%, respectively. This was because the pre-cracked beams all reached the stabilized load under the control displacement of 6 mm. Their span deflection was the same, and the number of cracks was similar, so their crack depths did not change much. While with the increase of the pre-cracked width, the residual cracks increased, the degree of seawater corrosion increased, and the material damage increased, resulting in decrease in the span deflection and crack depth at L_u.

From Table 4, the maximum crack width of beams after soaking in simulate seawater for one year more than that no-corrosion beams at L_{cr}, and with the increase of the BFRP reinforcement ratio, the gap of crack width between the two decreased. The crack width of beam with BFRP reinforcement ratio of 0.56% had doubled after being corroded by seawater, however, the crack width of beam with BFRP reinforcement ratio of 1.65% had not changed after being corroded by seawater. This was because that seawater corrosion reduced the tensile strength of concrete, made it easier to produce and develop cracks, in addition, the increase in the BFRP reinforcement ratio was conducive to inhibiting the generation of cracks. What's more, steel fiber in the concrete can effectively inhibit the development of cracks. According to the ACI 440.1R-15 code (ACI Committee, 2015), outdoor FRP-RC structures allow for a maximum crack width of 0.5 mm, while indoor structures allow for a maximum crack width of 0.7 mm. The maximum crack widths of SFRC beams with BFRP bars under L_s were less than the 0.5 mm recommended by the codes. Steel fiber were randomly distributed in the concrete matrix, and the steel fibers that had not been pulled out at the cracks could bear part of the tensile stress, thus reducing the tensile stress of the BFRP bars, the deformation of the beams and the width of

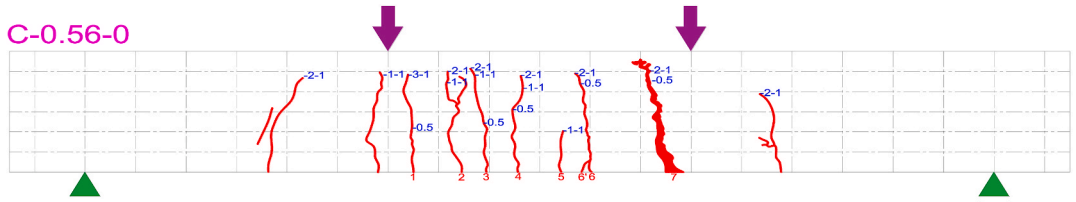

(a) Beam C-0.56-0

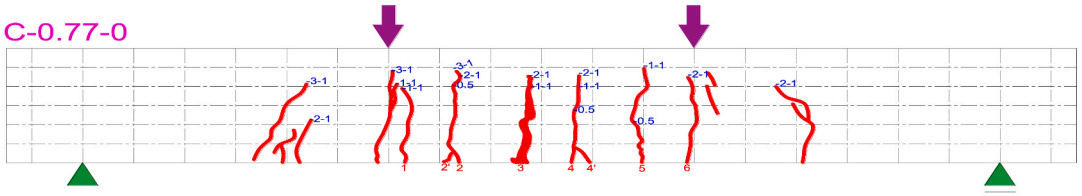

(b) Beam C-0.77-0

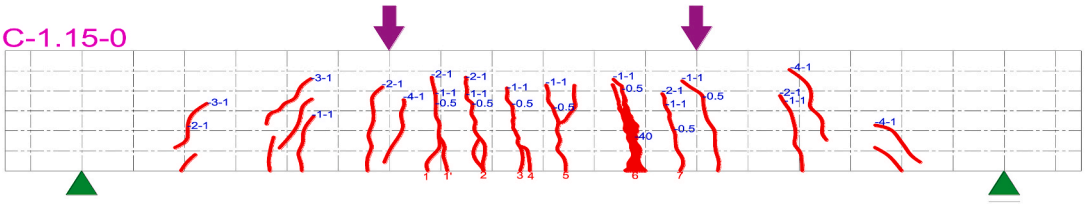

(c) Beam C-1.15-0

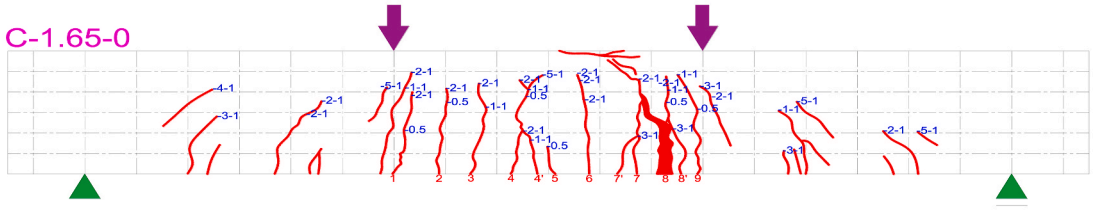

(d) Beam C-1.65-0

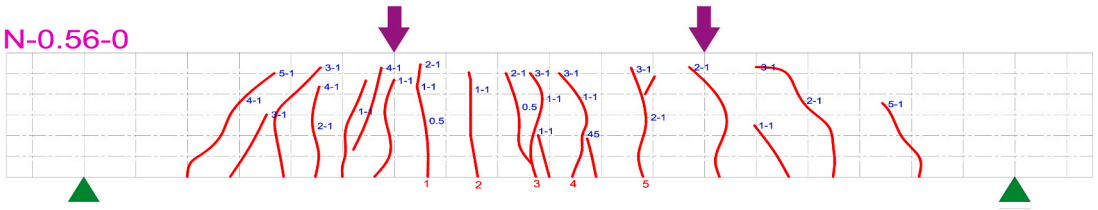

(e) Beam N-0.56-0

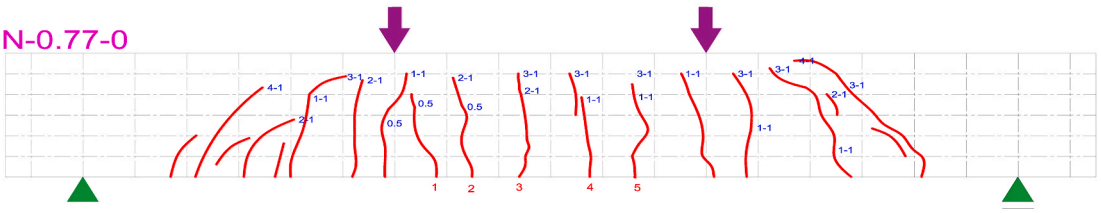

(f) Beam N-0.77-0

Fig. 7. Final crack distribution of the beams.

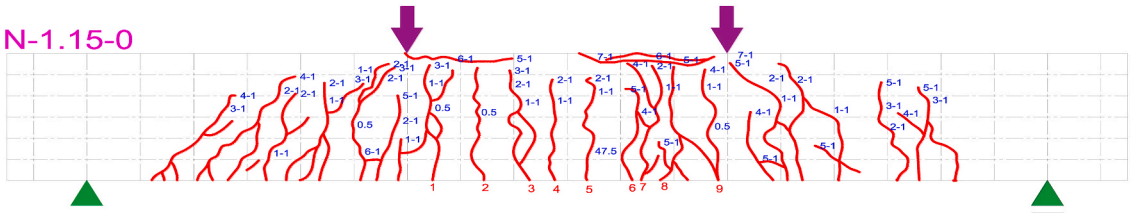

(g) Beam N-1.15-0

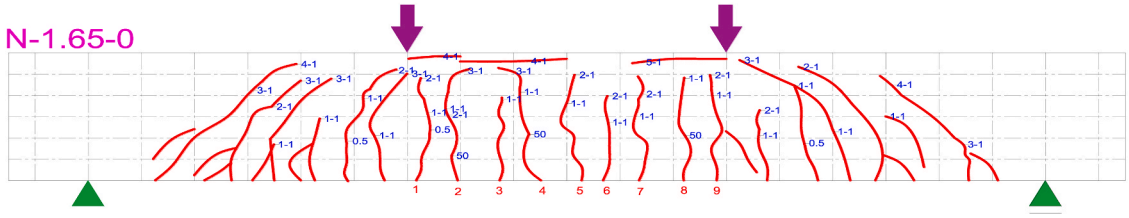

(h) Beam N-1.65-0

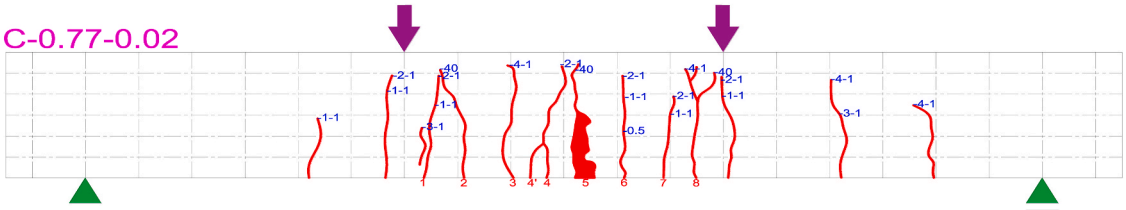

(i) Beam C-0.77-0.02

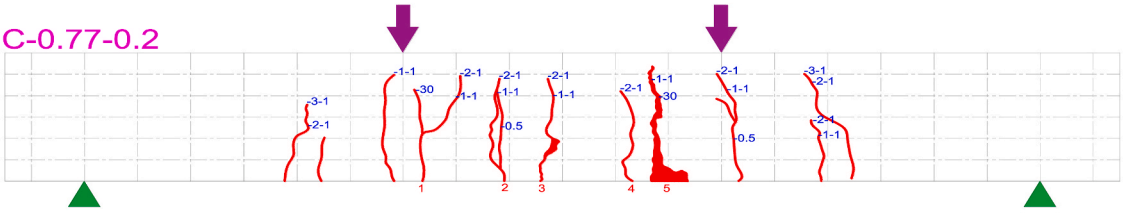

(j) Beam C-0.77-0.2

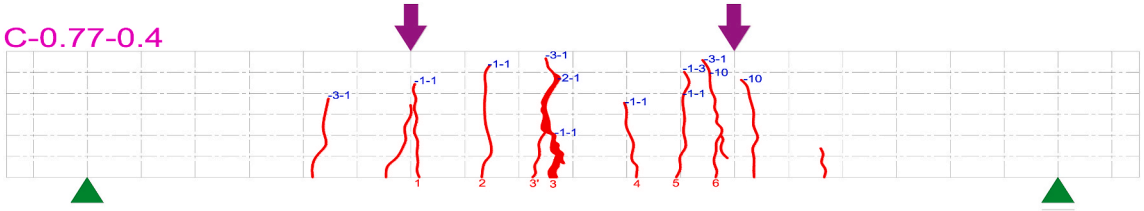

(k) Beam C-0.77-0.4

Fig. 7. (*continued*).

the cracks. The maximum crack widths of corrosion beams were less than that of no-corrosion beams at L_{st} and L_u, the maximum crack width of corrosion beam C-1.65-0 reduced by 33.3% and 55.2% comparing with no-corrosion beam N-1.65-0, respectively. From the load analysis of the previous section, it can be seen that the stabilized loads and ultimate loads of the no-corrosion beams were higher than that of the corrosion beams, so the span deflections of no-corrosion beams were greater, the strain of BFRP bars were increased, and the maximum crack width were wider.

3.3. Load vs. maximum crack width curves

Fig. 8 depicted the load vs. maximum crack width curves for SFRC beams with BFRP bars. There was a positive correlation between applied load and maximum crack width, and they all exhibited nonlinear characteristics. The stiffness of beams was the biggest before the cracking, while with the increase of load, the cracks occurred and extended continuously, resulting in a decrease in the effective load of inertia and decrease in stiffness of the beams, which made the strain of

Table 5
Load ratios under various crack widths.

Specimens	P	Crack widths (mm)							Average
		0.1	0.2	0.3	0.4	0.5	0.6	0.7	
C-0.56-0	P_{12}	1.00	0.98	0.96	0.95	0.94	0.93	0.94	0.96
	P_{13}	1.00	0.97	0.95	0.93	0.92	0.90	0.87	0.93
C-0.77-0	P_{12}	0.98	0.96	0.94	0.94	0.95	0.96	0.95	0.95
	P_{13}	0.97	0.94	0.92	0.91	0.92	0.93	0.92	0.93
C-1.15-0	P_{12}	0.99	0.98	0.97	0.95	0.95	0.94	0.96	0.96
	P_{13}	0.98	0.96	0.95	0.94	0.94	0.92	0.94	0.95
C-1.65-0	P_{12}	0.95	0.95	0.95	0.95	0.94	0.96	0.95	0.95
	P_{13}	0.93	0.92	0.93	0.93	0.93	0.95	0.92	0.93
C-0.77-0.02	P_{12}	0.93	0.93	0.93	0.93	0.94	0.94	0.94	0.93
	P_{13}	0.91	0.91	0.91	0.91	0.91	0.92	0.92	0.91
C-0.77-0.2	P_{12}	–	–	0.94	0.94	0.94	0.94	0.94	0.94
	P_{13}	–	–	0.94	0.93	0.93	0.91	0.91	0.92
C-0.77-0.4	P_{12}	–	–	–	–	0.95	0.95	0.92	0.94
	P_{13}	–	–	–	–	0.93	0.93	0.90	0.92
N-0.56-0	P_{12}	0.98	0.96	0.95	0.94	0.93	0.93	0.93	0.94
	P_{13}	0.98	0.95	0.93	0.91	0.90	0.90	0.91	0.93
N-0.77-0	P_{12}	1.00	1.00	1.00	0.99	0.97	0.96	0.94	0.98
	P_{13}	0.97	0.93	0.90	0.88	0.90	0.91	0.93	0.92
N-1.15-0	P_{12}	0.97	0.94	0.93	0.93	0.94	0.94	0.95	0.94
	P_{13}	1.04	0.96	0.90	0.91	0.92	0.93	0.93	0.94
N-1.65-0	P_{12}	0.99	0.98	0.96	0.95	0.95	0.95	0.95	0.96
	P_{13}	0.98	0.97	0.96	0.94	0.94	0.94	0.94	0.95
Average	P_{12}	0.98	0.96	0.95	0.95	0.95	0.94	0.94	0.95
	P_{13}	0.97	0.94	0.93	0.92	0.92	0.92	0.92	0.93
Standard deviation		0.03	0.02	0.02	0.02	0.02	0.02	0.02	0.03

FRP bars more pronounced with the change in load in the later stage, accelerating the growth rate of crack width. Another reason was that the position of the crack corresponding to the maximum crack width was not fixed, it may change with the increase of the load.

More importantly, the peak load of beams decreased with the increase of the number of loading cycles under the same deflection, while the degradation rate decreases with higher cyclic number. As shown in Table 5, the P_{13} was always less than P_{12}, and the difference between P_{11} and P_{12} was greater than the difference between P_{12} and P_{13}. Where P is the ratios of the load of second and third loading to the first loading under different maximum crack widths of the beams. The P_{12} is the ratios of the second loading to the first loading, and the P_{13} is the ratios of third loading to first loading. One of the reasons was that the specimens had a plastic deformation after cracking, and irreparable residual cracks may appear after unloading, so that the maximum crack width of the beams increased with the increase of the number of loading cycles. Another reason was that the cracks of the beams during the first loading cycle developed rapidly, and the maximum crack width improved greatly. And the increase of maximum crack width in the second and third loading were only related to the cumulative damage of concrete and BFRP bars. Therefore, the changes of crack width in the second and third loading were smaller than that in the first loading.

From Table 5 and it could be observed that the bearing capacity degradation of all SFRC beams with BFRP bars after three loading and unloading cycles were less than 10% when the maximum crack width was less than 0.7 mm. Therefore, when calculating the maximum crack width of SFRC beams with BFRP bars under cyclic loading, a cyclic loading influence factor "λ" recommended introducing, where "λ" is taken as 1.1. In addition, the cyclic loading had the greatest impact on the maximum crack width of pre-cracked beams after seawater corrosion, while it had the smallest impact on non-corrosion beams.

3.4. Load vs. maximum crack width curves under the first loading and unloading

Fig. 9 illustrated the load-maximum crack width curves for all beams with different variables under the first loading-unloading cycle. The slope of the load-maximum crack width curves of experimental beams increased with a higher BFRP reinforcement ratio and a smaller pre-cracked width. When the load value was $0.3M_u$, for beam N-0.77-0, increasing the reinforcement ratio by 49% and 114% at L_s would reduce the maximum crack widths by 33% and 67%, respectively, while reducing the reinforcement ratio by 27% would increase the maximum crack width by 73%. Similar results were observed for corroded beams. For beam C-0.77-0, increasing the reinforcement ratio by 49% and 114% at L_s resulted in a reduction of crack width by 50% and 80%, respectively, while a 27% reduction in reinforcement ratio led to a 150% increase in maximum crack width. The reason was that increasing the BFRP reinforcement ratio would improve the bonding capacity between the concrete and the BFRP bars, which could inhibit the development of cracks. When the load value was $0.3M_u$, for beam N-0.77-0, increasing the pre-cracked width to 0.02 mm, 0.2 mm, 0.4 mm resulted in a reduction of crack width by 73%, 153% and 247%, respectively. This was because the pre-cracked width increased, resulting in an increase in the initial residual crack of the tested beams, a decrease in the energy required for crack expansion, so the cracks were easier to extend. Therefore, with the increase of pre-cracked width, the maximum crack width of SFRC beams with BFRP bars increased. Everyone knows that seawater corrosion caused damage to the BFRP bars and concrete, causing a decrease in the strength of the beams, which in turn led to a decrease in the slope of the load-crack width curve. However, the corrosion beams in this study were cured for 365d, and the no-corrosion beams were only cured for 28d, resulting an increase of concrete strength, as a result, and the maximum crack widths of the corrosion beams with BFRP reinforcement ratios of 0.77%, 1.15% and 1.65% under the same load were less than that of the no-corrosion beams.

4. Theoretical study on crack width

4.1. Models recommended by codes

Table 6 lists the calculation models for the maximum crack width of FRP-RC beams in existing codes.

Eg: f_f is the stress of FRP bars; E_f is the elastic modulus of FRP bar; β is the ratio of the distance from the neutral axis to the edge of the tensile zone of the beams section and the distance from the neutral axis to the centroid of the tension bar; κ_b is the correction coefficient for bonding performances, which is taken as 1.4 when there is no experimental data

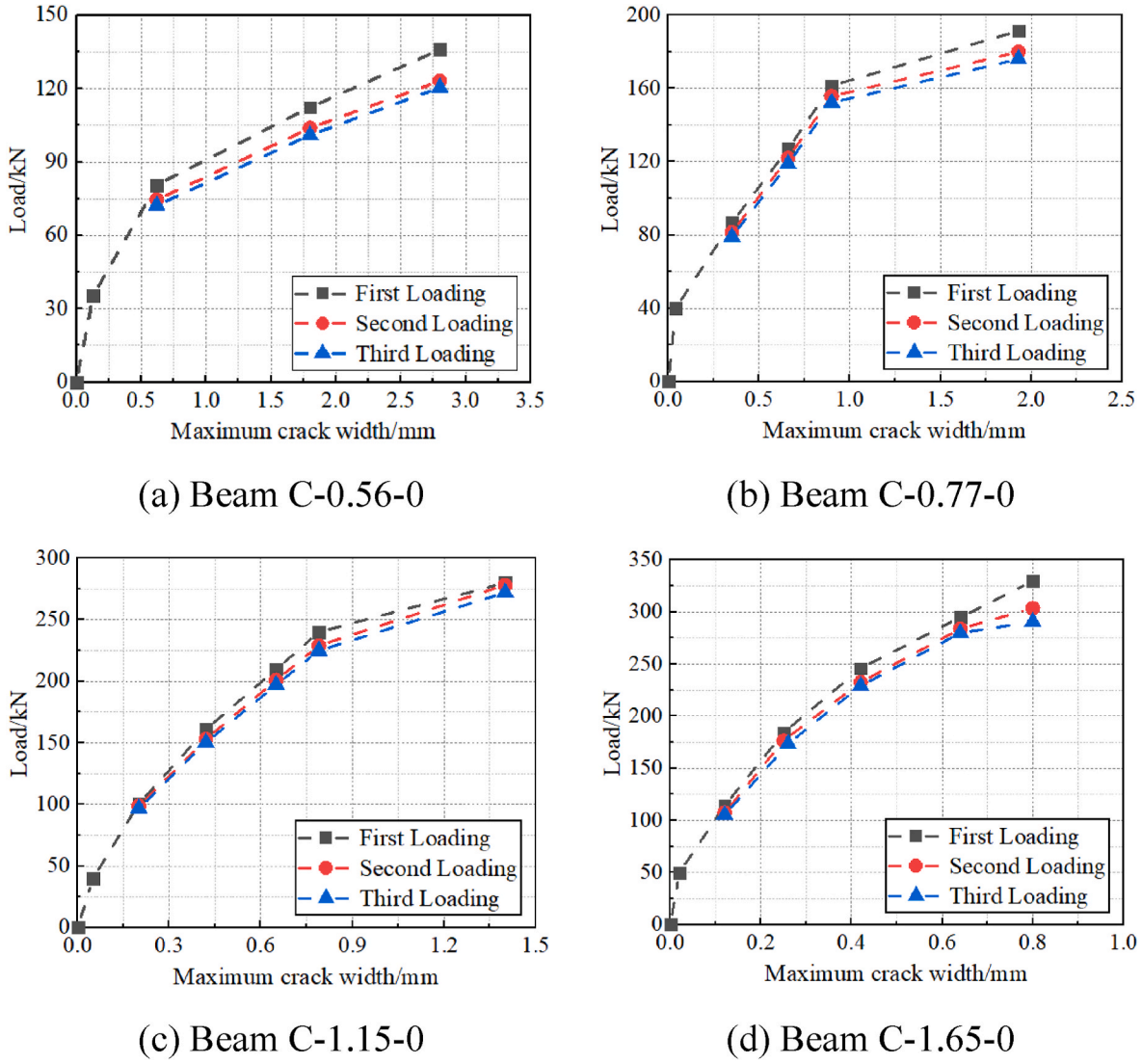

Fig. 8. Load vs. maximum crack width curves of beams.

(Abed (Dong et al., 2018) and Ahmed (Mohamed et al., 2021) found that the correction coefficient of BFRP bars can be taken as 0.7 or 0.8.); s is the bar spacing; d_c is the concrete cover; ψ is the strain non-uniformity coefficient of FRP bar; φ is the effective reinforcement ratio of FRP bars; ρ_{te} is the longitudinal tensile reinforcement ratio; k is a constant expressing the effects of bond characteristics and multiple placements of reinforcement materials.

4.2. New prediction model

Unlike RC beams, SFRC beams have randomly distributed steel fibers, which can improve the tensile strength of concrete and suppress the development of cracks. More importantly, SFRC in the tensile zone still had a certain residual strength after cracking to resist crack propagation (Feng et al., 2021; Zhang et al., 2023). However, the calculation models for crack width in FRP-RC beams in existing codes did not consider the inhibitory effect of steel fibers on crack propagation. To this end, this study considered the effect of SFRC on the crack width of FRP-RC beams and proposed a new calculation model for the crack width of SFRC beams with BFRP bars.

Fig. 10 illustrates the cross-sectional area, strain, and stress distribution of SFRC beams with BFRP bars under normal service states. As the cracks continued to expand, some steel fibers were gradually pulled or pulled out during the loading process, resulting in the stress borne by the steel fibers being continuously transferred to the BFRP bars. As such, it can be assumed that the stress of steel fibers was highest at the neutral axis, and zero at the bottom of the section. In SFRC beams, prior to the appearance of cracks in the tension zone of concrete, BFRP bars and steel fibers were responsible for bearing all tensile stress at the crack location. The randomly distributed steel fibers also contribute to resisting cracking. However, the ACI 440.1 R model (ACI Committee, 2015) does not consider the contribution of steel fibers in reducing crack width. Therefore, this study proposed a calculation model for the crack width of SFRC beams with FRP bars based on the stress characteristics of SFRC sections.

Based on the principles of strain compatibility, force equilibrium, and bending moment equilibrium, the stress (f_f) of BFRP bars in the beams can be determined using the following equation.

$$\frac{E_c \varepsilon_c bc}{2} = f_f A_f + \frac{f_{sf} b(h-c)}{2} \tag{11}$$

$$\frac{\varepsilon_c}{\varepsilon_{sf}} = \frac{2c}{h-c} \tag{12}$$

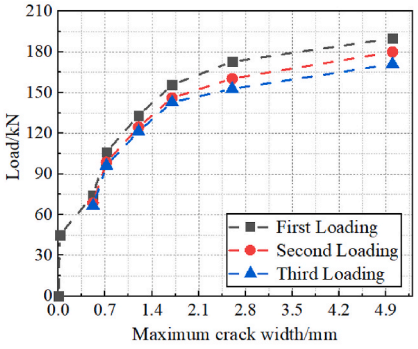

(e) Beam N-0.56-0

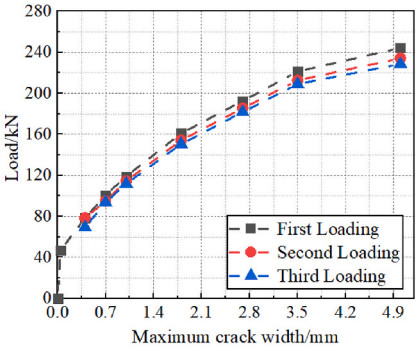

(f) Beam N-0.77-0

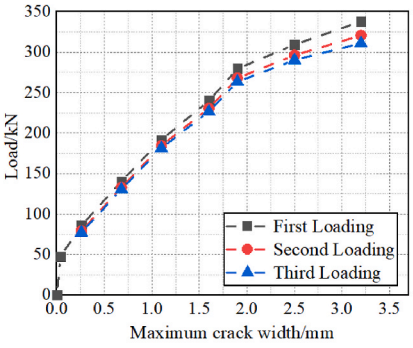

(g) Beam N-1.15-0

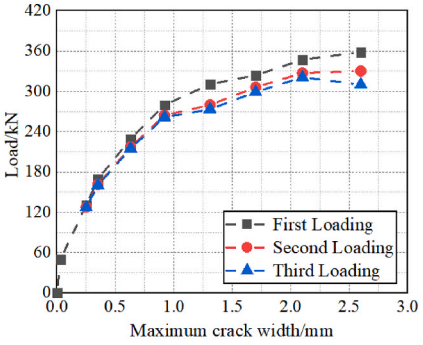

(h) Beam N-1.65-0

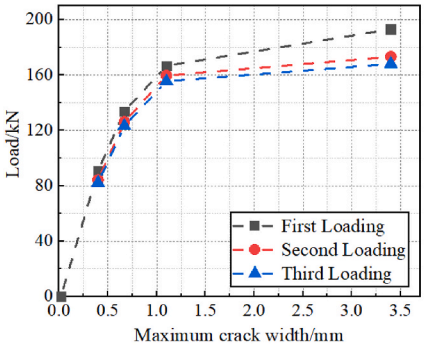

(i) Beam C-0.77-0.02

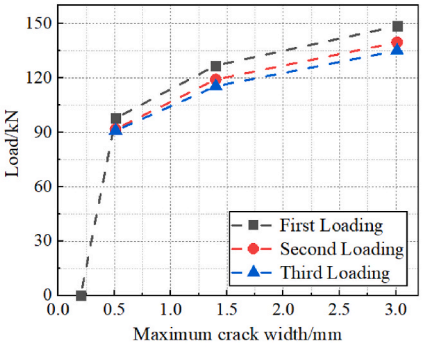

(j) Beam C-0.77-0.2

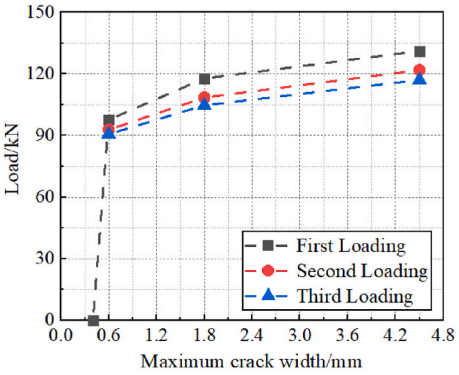

(k) Beam C-0.77-0.4

Fig. 8. (*continued*).

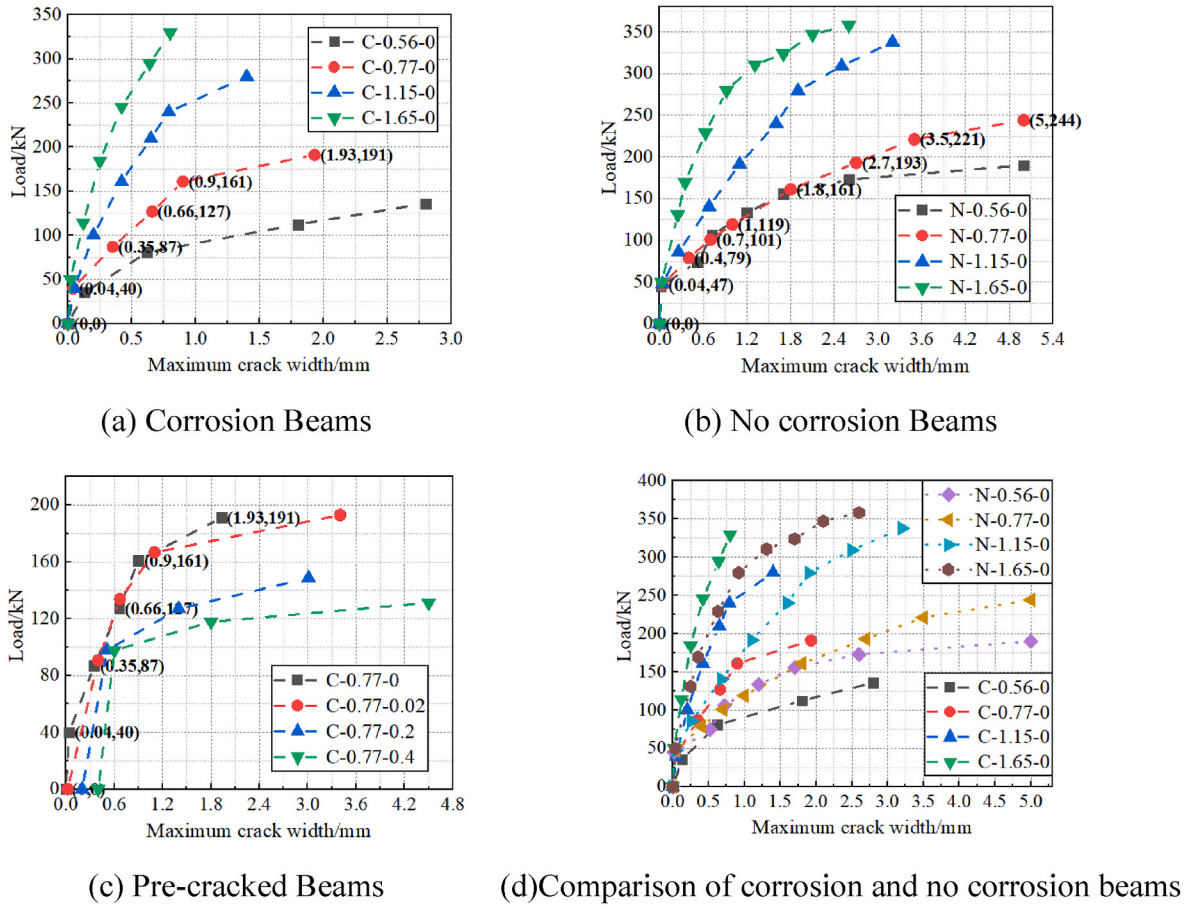

Fig. 9. Load vs. maximum crack width curves under the first loading and unloading.

$$0.3M_u = f_f A_f \left(d - \frac{c}{3}\right) + \frac{f_{sf} b(h-c)}{6}(h+c) \tag{13}$$

$$f_f = \frac{0.3M_u - \frac{f_{sf} b(h-c)}{6}(h+c)}{A_f\left(d - \frac{c}{3}\right)} \tag{14}$$

The residual strength (f_{sf}) of SFRC after cracking can be evaluated using the calculation foemula proposed by Zhang (Zhang et al., 2016).

$$f_{sf} = \frac{1}{3}\alpha\tau_f V_{sf}(1+f)\left(1+\frac{1}{2}\omega_2\right)\left(1-\frac{kw}{l_{sf}}\right) \tag{15}$$

where α is the aspect ratio of fibers; τ_f is the average bond strength; V_f is the volume fraction of steel fibers; f is the coefficient of friction between concrete and fiber sheared over the crack edge; ω_2 is the degree of planar orientation of fibers; k is 8 or 4, for straight or hooked-end fibers, respectively; ω is the average crack width; l_f is the ratio between fiber length and fiber diameter.

Based on the calculation method for crack width of FRP-RC beams in ACI 440.1R-15 (ACI Committee, 2015) code, Eq. (16) can be obtained by incorporating Eq. (14) into Eq. (15).

$$\omega_{\max} = 2E_f \beta\kappa_b \sqrt{d_c^2 + \left(\frac{s}{2}\right)^2}\ \frac{0.3M_u - \frac{1}{18}b\alpha\tau_f V_f(1+f)\left(1+\frac{1}{2}\omega_2\right)\left(1-\frac{kw}{l_f}\right)(h^2-c^2)}{A_f\left(d-\frac{c}{3}\right)} \tag{16}$$

$$\kappa_b = 0.9 \tag{17}$$

However, the maximum crack width of the beams increased by 11% after one year of erosion under service load. Other studies (Marcos-Meson et al., 2018) showed that soaking SFRC beams in simulated seawater solution can increase the crack width under the same loading. Therefore, it is necessary to consider the impact of erosion environment on the maximum crack width of beams. Based on the research results, the crack widths of corroded beams under seawater environments were analyzed and fitted. The average ratio between the calculated and actual results of the maximum crack width of the corroded beams using Eq. (16) was 1.10. For pre-cracked beams, the value of κ_b was closely related to the pre-cracked width. Fit existing test data, κ_b can be calculated using the following equation.

$$\kappa_b = 0.9 + \omega_{pre-crack} \tag{18}$$

where $\omega_{\text{pre-crack}}$ is the pre-cracked width of beams.

Table 6
The calculation models for the maximum crack width of FRP-RC beams in existing codes.

Codes	Calculation models
ACI 440.1R-15 code (ACI Committee, 2015)	$\omega_{max,ACI} = 2\frac{f_f}{E_f}\beta\kappa_b\sqrt{d_c^2+\left(\frac{s}{2}\right)^2}$
GB 50608-2010 (Technical code for infrastructure application, 2010)	$\omega_{max,GB} = 2.1\psi\frac{f_f}{E_f}\left(1.9d_c + 0.08\frac{\varphi}{\rho_{te}}\right)$
JSCE-97 b (Recommendation for design and construction, 1997)	$\omega_{max,JSCE} = k[4d_c + 0.7(s-\varphi)]\frac{f_f}{E_f}$

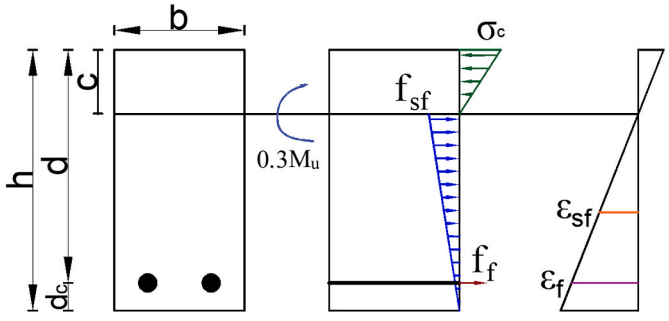

Fig. 10. Analysis for a SFRC section under flexural bending.

4.3. Crack width of SFRC beams from experiment and various analytical models

Table 7 lists the comparison between the experimental and calculated values of crack width under service load. From Table 7, the calculation results of ACI 440.1R-15 (ACI Committee, 2015), GB 50608-2010 (Technical code for infrastructure application, 2010), and JSCE-97 b (Recommendation for design and construction, 1997) for the maximum crack width of beams were 63%, 245%, and 74% larger than the experimental results, respectively. This is mainly because the existing codes did not consider the inhibitory effect of steel fibers on crack propagation. On the contrary, the results of the maximum crack width using the new calculation model proposed in this study were very consistent with the experimental results, and the average ratio of the calculated results to the actual results was only 1.1 under service load. Fig. 11 presents the experimental crack width values and calculated crack width values for each beam under service load. From Fig. 11, it can be observed that compared with other calculation methods, the crack width calculation model proposed in the study was closest to the experimental results.

5. Conclusions

This paper aimed to evaluate the cracking behavior of SFRC beams with BFRP bars corroded by seawater under cyclic loading. Eleven SFRC beams with BFRP bars were poured and tested through a four-point bending tests under cyclic loading. Based on experimental variables, they were divided into three groups, including corroded, no-corroded, and pre-cracked. The load, crack initiation and propagation, crack depth, and crack width of the SFRC beams with BFRP bars were recorded and analyzed during the experiment. Furthermore, a calculation model for the crack width of SFRC beams with BFRP bars under corrosion and cyclic loading was established, verified, and compared with experimental results and predictions from formulae in ACI440.1R-15, GB 50608-2010, and JSCE-97 b. Our investigation led to the following conclusions:

1. There was a significant degradation in the tensile strength of BFRP bars after soaking in simulated seawater solution for 1 year, and the strength degradation rates of the reference BFRP bars increased with the increase of the diameter of BFRP bars. The tensile strength of BFRP bars with a diameter of 14 mm after seawater corrosion was reduced by 11.2%. But the difference was that the compressive strength of SFRC had increased by 15.9% after seawater corrosion.
2. Two failure modes of beams were observed in the experiment, including compression failure (CF) and BFRP bars tensile failure (TF). Most notably, the failure mode of the beams changed from CF to TF after seawater corrosion under the same BFRP reinforcement ratios.
3. The maximum crack widths of all SFRC beams with BFRP bars under service load was less than the 0.5 mm recommended by the ACI 440.1R-15 code. In addition, the peak load of beams decreased with the increase of the number of loading cycles under the same deflection, while the degradation rate decreased with higher cyclic numbers. The bearing capacity degradation of all beams after three loading and unloading cycles were less than 10% when the maximum crack width was less than 0.7 mm.
4. For beams corroded by seawater or under natural conditions, increasing the BFRP reinforcement ratios can increase the number of cracks, reduce the crack depth and the maximum crack width under a certain load, but its impact on the cracking load was not significant. For beam C-0.77-0, increasing the BFRP reinforcement ratio by 114% would reduce the maximum crack widths by 80% at service load.
5. The pre-cracked width has an adverse impact on the crack control of beams, with the increase of pre-cracked width from 0 to 0.02 mm, 0.2 mm and 0.4 mm, the ultimate load decreased by 1.5%, 20.6% and 48.5%, the crack depth increased by 10%, 9% and 14% at ultimate load, the crack width increased by 73%, 153% and 247%, respectively.
6. Seawater erosion has an obvious impact on the flexural behaviors of beams, the crack load, stabilized load and ultimate load of beams had

Table 7
Comparison between the actual and calculated values of crack width under service load.

Specimen	$\omega_{max,act}$	$\omega_{max,pro}$	$\omega_{max,pro}/\omega_{max,\ act}$	$\omega_{max,ACI}$	$\omega_{max,ACI}/\omega_{max,\ act}$	$\omega_{max,GB}$	$\omega_{max,GB}/\omega_{max,\ act}$	$\omega_{max,JSCE}$	$\omega_{max,JSCE}/\omega_{max,\ act}$
C-0.56-0	0.36	0.39	1.11	0.61	1.72	1.50	4.22	0.64	1.81
C-0.77-0	0.36	0.37	1.03	0.58	1.60	1.32	3.68	0.61	1.70
C-1.15-0	0.31	0.31	0.99	0.48	1.54	0.93	3.00	0.53	1.70
C-1.65-0	0.29	0.37	1.27	0.57	1.98	0.85	2.95	0.60	2.07
C-0.77-0.02	0.37	0.38	1.04	0.58	1.58	1.33	3.64	0.61	1.68
C-0.77-0.2	0.32	0.38	1.18	0.48	1.51	1.11	3.47	0.51	1.60
C-0.77-0.4	0.35	0.37	1.03	0.39	1.11	0.91	2.56	0.42	1.18
N-0.56-0	0.38	0.46	1.22	0.72	1.90	1.78	4.67	0.76	2.00
N-0.77-0	0.40	0.47	1.18	0.73	1.83	1.69	4.21	0.78	1.94
N-1.15-0	0.38	0.40	1.06	0.63	1.65	1.23	3.23	0.69	1.82
N-1.65-0	0.40	0.40	1.00	0.62	1.55	0.93	2.31	0.65	1.62
Average value	0.36	0.39	1.10	0.58	1.63	1.23	3.45	0.62	1.74
Mean squared			0.09		0.22		0.70		0.23

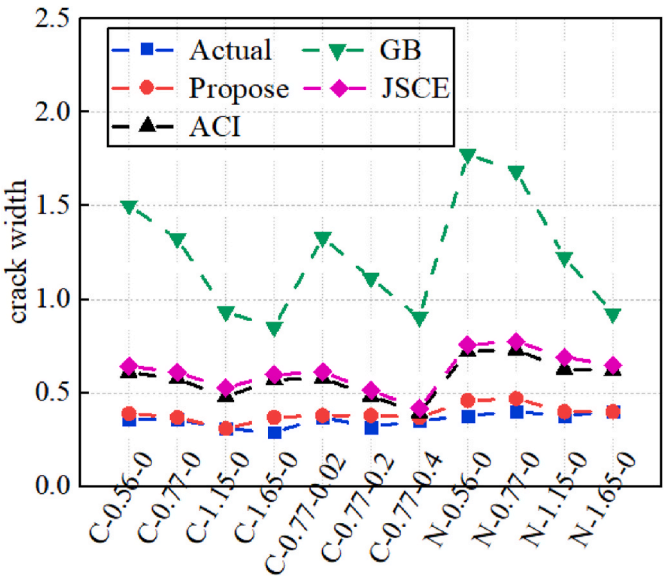

Fig. 11. Contrast of model calculation results.

a reduction after soaking in simulated seawater solution for 1 year, but the crack depth of beams increased. In addition, the influence of flexural behaviors on the beams with low BFRP reinforcement ratio was higher than that of beams with high BFRP reinforcement ratio.

7. The crack widths of BFRP-SFRC beams were overestimated by the ACI 440.1R-15, GB 50608-2010, and JSCE-97 b models, as found through a comparison with experimental results. Thus, a value of 0.9 for the coefficient κ_b of the analytical model recommended by ACI should be adopted, taking into account the effects of steel fibers, corrosion, and repeated loading. In addition, the effect of pre-cracked can be accounted for by adopting the value of $\kappa_b = 0.9+\omega_{pre\text{-}crack}$. The proposed model provided results closer to the actual outcome compared with ACI 440.1R-15, GB 50608-2010, and JSCE-97 b models.

CRediT authorship contribution statement

Haitang Zhu: Investigation, Writing-review & editing, Conceptualization, Supervision. Wencheng Duan: Investigation, Data curation, Writing-original draft, Writing-review & editing. Zongze Li: Writing-review & editing, Supervision, Methodology. Zemin Li: Investigation, Data curation. Xiangming Zhou: Writing-review & editing; Supervision. Qingxin Meng: Investigation, Data curation.

Declaration of competing interest

The authors declare that they have no known competing financial interests or personal relationships that could have appeared to influence the work reported in this paper.

Data availability

Data will be made available on request.

Acknowledgements

This research work was financially supported by the Natural Science Foundation of Henan Province (No.232300420102), National Natural Science Foundation of China (No. 52378234), the Science and Technology Research and Development Project of CSCEC (under the grant No. CSCEC-2021-Z-24), the Postdoctoral Research Foundation of China (No. 2023TQ0298), Key scientific research projects in higher education institutions in Henan Province (24B570002) and the Qiushi Research Initiation Foundation of Zhengzhou University (No. 32213572-22).

References

ACI Committee, 2012. Guide Test Methods for Fiber Reinforced Polymer (FRP) Composites for Reinforcing or Strengthening Concrete and Masonry Structures. America: ACI.
ACI Committee, 2015. 1R15: Guide for the Design and Construction of Concrete Reinforced with FRP Bars. American Concrete Institute (ACI) Committee, 440.
Ali, A.H., Mohamed, H.M., Benmokrane, B., 2020. Bar size effect on long-term durability of sand-coated basalt-FRP composite bars. Compos. B Eng. 195, 108059.
Almusallam, H. Tarek, Al-Salloum, Yousef, A., 2006. Durability of GFRP rebars in concrete beams under sustained loads at severe environments. J. Compos. Mater. 40 (7), 623–637.
Benmokrane, B., Manalo, A., Bouhet, J.C., Mohamed, K., Robert, M., 2017. Effects of diameter on the durability of glass fiber–reinforced polymer bars conditioned in alkaline solution. J. Compos. Construct. 21 (5), 04017040.
Demis, S., Papadakis, V.G., 2019. Durability design process of reinforced concrete structures - service life estimation, problems and perspectives. J. Build. Eng. (26), 100876
Deng, Z.H., Zhong, X.G., Liu, B., et al., 2022. Study on flexural behavior of coral concrete beams reinforced with CFRP bars. Structures (39), 378–386.
Dong, Z.Q., Wu, G., Zhao, X.L., Zhu, H., Lian, J.L., 2018. Durability test on the flexural performance of seawater sea-sand concrete beams completely reinforced with FRP bars. Construct. Build. Mater. 192, 671–682.
Dong, Z.Q., Wu, G., Zhu, H., Zhao, X.L., Wei, Y., Qian, H., 2020. Flexural behavior of seawater sea-sand coral concrete–UHPC composite beams reinforced with BFRP bars. Construct. Build. Mater. (265), 120279
Dong, Z.Q., Sun, Y., Zhu, H., Wu, G., Shao, X.X., 2022. Shear behavior of hybrid seawater sea-sand concrete short beams reinforced with BFRP reinforcements. Eng. Struct. (252), 113615
Feng, Z., Li, C.X., Yoo, D.Y., Pan, R.S., He, J., Ke, L., 2021. Flexural and cracking behaviors of reinforced UHPC beams with various reinforcement ratios and fiber contents. Eng. Struct. 248, 113266.
Feng, G.Y., Zhu, D.J., Guo, S.C., Rahman, M.Z., Jin, Z.Q., Shi, C.J., 2022. A review on mechanical properties and deterioration mechanisms of FRP bars under severe environmental and loading conditions. Cement Concr. Compos. 134, 104758.
Gribniak, V., Sokolov, A., 2023. Standardized RC beam tests for modeling the fiber bridging effect in SFRC. Construct. Build. Mater. (370), 130652
Guo, X.K., Jin, Z.Q., Xiong, C.S., et al., 2022. Deterioration of mechanical properties of basalt/carbon hybrid FRP bars in SWSC under seawater corrosive environment. Construct. Build. Mater. (317), 125979
Hamed, F., Matteo, D.B., Cristina, M.O., et al., 2018. Long-term performance of GFRP bars in concrete elements under sustained load and environmental actions. Compos. Struct. 190, 20–31.
He, X.J., Dai, L., Yang, W.R., 2017. Durability and degradation mechanism of GFRP bars embedded in concrete beams with cracks. Plast., Rubber Compos. 46 (1), 17–24.
Hollaway, L.C., 2010. A review of the present and future utilisation of FRP composites in the civil infrastructure with reference to their important in-service properties. Construct. Build. Mater. 24 (12), 2419–2445.
Hou, L.J., Peng, Y.H., Xu, R., Zhang, X.F., Huang, T., Chen, D., 2021. Corrosion behavior and flexural performance of reinforced SFRC beams under sustained loading and chloride attack. Eng. Struct. (242), 112553
Hu, B., Zhou, Y.W., Xing, F., et al., 2019. Experimental and Theoretical Investigation on the Hybrid CFRP-ECC Flexural Strengthening of RC Beams with Corroded Longitudinal Reinforcement, vol. 200. Engineering Structures, 109717.
Li, S., Guo, S.C., Yao, Y., Jin, Z.Q., Shi, C.J., Zhu, D.J., 2021. The effects of aging in seawater and SWSSC and strain rate on the tensile performance of GFRP/BFRP composites: a critical review. Construct. Build. Mater. (282), 122534
Li, S.C., Jin, Z.Q., Pang, B., Li, J.Q., 2022. Durability performance of an RC beam under real marine all corrosion zones exposure for 7 years. Case Stud. Constr. Mater. (17), e01516
Liang, X.Z., Yin, S.P., Hu, C.S., 2021. Environmental reduction factors of BFRP bars in coral aggregate concrete in high temperature and high humidity environments. Structures (33), 3017–3024.
Liu, J., Lei, Y.S., Yu, W.X., et al., 2021. Dynamic shear failure and size effect in BFRP-reinforced concrete deep beam. Eng. Struct. (245), 112951
Lu, Z.Y., Li, W.K., Zeng, X.Y., Pan, Y.F., 2023a. Durability of BFRP bars and BFRP reinforced seawater sea-sand concrete beams immersed in water and simulated seawater. Construct. Build. Mater. (363), 129845
Lu, Z.Y., Li, W.K., Zeng, X.Y., Pan, Y.F., 2023b. Durability of BFRP bars and BFRP reinforced seawater sea-sand concrete beams immersed in water and simulated seawater. Construct. Build. Mater. 363, 129845.
Marcos-Meson, V., Michel, A., Solgaard, A., Fischer, G., Edvardsen, C., Skovhus, T.L., 2018. Corrosion resistance of steel fibre reinforced concrete - a literature review. Cement Concr. Res. 103, 1–20.
Mohamed, O.A., Hawat, W.A., Keshawarz, M., 2021. Durability and mechanical properties of concrete reinforced with basalt fiber-reinforced polymer (BFRP) bars: towards sustainable infrastructure. Polymers 13 (9), 1402.
Ngo, T.T., Pham, T.M., Hao, H., 2020. Effects of steel fibres and prestress levels on behaviour of newly proposed exterior dry joints using SFRC and CFRP bolts. Eng. Struct. (205), 110083
Recommendation for Design and Construction of Concrete Structures Using Continuous Fiber Reinforcing Materials, 1997. Japan Society of Civil Engineers (JSCE), Japan.

Ribeiro, S.E.C., Diniz, S.M.C., 2013. Reliability-based design recommendations for FRP-reinforced concrete beams. Eng. Struct. (52), 273–283.
Standard, C.S.A., 2012. Design and Construction of Building Structures with Fiber-Reinforced Polymers. CAN, CSA S806–12. Canadian Standards Association.
Standard Practice for Preparation of Substitute Ocean Water. ASTM D11412014.
Su, C., Wang, X., Ding, L.N., Wu, Z.S., Ma, X.G., 2022a. Durability of seawater sea sand concrete beams reinforced with carbon nanotube-modified BFRP bars in a marine environment. Compos. Struct. 292, 115642.
Su, C., Wang, X., Ding, L.N., Wu, Z.S., Ma, X.G., 2022b. Durability of seawater sea sand concrete beams reinforced with carbon nanotube-modified BFRP bars in a marine environment. Compos. Struct. 292, 115642.
Technical Code for Infrastructure Application of FRP Composites, 2010. Standards Press of China.
Technical specification for fiber reinforced concrete structures. CECS 38, 2004, 2004.
Wang, Z., Zhao, X.L., Xian, G.J., Wu, G., Raman, R.K.S., Al-Saadi, S., 2018. Effect of sustained load and seawater and sea sand concrete environment on durability of basalt- and glass-fibre reinforced polymer (B/GFRP) bars. Corrosion Sci. 138, 200–218.
Wang, L., Fan, L.B., Fu, F., Song, Z.P., 2022. Cracks width prediction of steel-FRP bars reinforced high-strength composite concrete beams. Structures 43, 424–433.
Wang, Z.H., Xie, J.H., Mai, Z.H., Liu, P., Lu, Z.Y., Li, L.J., 2023. Durability of GFRP bar-reinforced seawater–sea sand concrete beams: coupled effects of sustained loading and exposure to a chloride environment. Eng. Struct. (283), 115814
Wu, W.W., He, X.G., Yang, W.R., Dai, L., Wang, Y.G., He, J., 2022. Long-time durability of GFRP bars in the alkaline concrete environment for eight years. Construct. Build. Mater. 314, 125573.
Wu, C., Ma, G., Hwang, H.J., 2023. Bond performance of spliced GFRP bars in pre-damaged concrete beams retrofitted with CFRP and UHPC. Eng. Struct. (292), 116523
Xiao, S.H., Lin, J.X., Li, L.J., et al., 2021. Experimental study on flexural behavior of concrete beam reinforced with GFRP and steel-fiber composite bars. J. Build. Eng. (43), 103087
Yuan, T., 2019. Influence of Natural Exposure on Flexural Property of FRP Rods and Concrete Beams Made of Seawater and Sea Sand. Guangzhou University, Guangzhou.
Zhang, F.S., Ding, Y.N., Xu, J., Zhang, Y.L., Zhu, W.Q., Shi, Y.X., 2016. Shear strength prediction for steel fiber reinforced concrete beams without stirrups. Eng. Struct. 127, 101–116.
Zhang, Y., Zhu, Y.P., Qiu, J.F., Hou, C.G., Huang, J.J., 2023. Impact of reinforcing ratio and fiber volume on flexural hardening behavior of steel reinforced UHPC beams. Eng. Struct. 285, 116067.
Zhu, H.T., Li, Z.Z., Wen, C.C., et al., 2020. Prediction model for the flexural strength of steel fiber reinforced concrete beams with fiber-reinforced polymer bars under repeated loading. Compos. Struct. (250), 112609